

1 **TITLE: The somatic genetic and epigenetic mutation rate in a wild long-lived**
2 **perennial *Populus trichocarpa***

3
4 **AUTHORS**

5
6 Brigitte T. Hofmeister¹, Johanna Denkena², Maria Colomé-Tatché^{2,3,4}, Yadollah
7 Shahryary⁵, Rashmi Hazarika^{5,6}, Jane Grimwood^{7,8}, Sujan Mamidi⁷, Jerry Jenkins⁷, Paul
8 P. Grabowski⁷, Avinash Sreedasyam⁷, Shengqiang Shu⁸, Kerrie Barry⁸, Kathleen Lail⁸,
9 Catherine Adam⁸, Anna Lipzen⁸, Rotem Sorek⁹, Dave Kudrna¹⁰, Jayson Talag¹⁰, Rod
10 Wing¹⁰, David W. Hall¹¹, Gerald A. Tuskan¹², Jeremy Schmutz^{7,8}, Frank Johannes^{5,6,*},
11 Robert J. Schmitz^{6,11,*}

12
13 ¹Institute of Bioinformatics, University of Georgia, Athens, GA, USA

14 ²Institute of Computational Biology, Helmholtz Center Munich, German Research
15 Center for Environmental Health, Neuherberg, Germany

16 ³European Research Institute for the Biology of Ageing, University of Groningen,
17 University Medical Centre Groningen, Groningen, The Netherlands

18 ⁴TUM School of Life Sciences Weihenstephan, Technical University of Munich, Freising,
19 Germany

20 ⁵Department of Plant Sciences, Technical University of Munich, Liesel-Beckmann-Str. 2,
21 Freising, Germany

22 ⁶Institute for Advanced Study (IAS), Technical University of Munich, Lichtenbergstr. 2a,
23 Garching, Germany

24 ⁷HudsonAlpha Institute of Biotechnology, Huntsville, Alabama, USA

25 ⁸Department of Energy Joint Genome Institute, Walnut Creek, California, USA

26 ⁹Department of Molecular Biology, Weizmann Institute of Science, Rehovot, Israel

27 ¹⁰Arizona Genomics Institute, School of Plant Sciences, University of Arizona, Tucson,
28 AZ, USA

29 ¹¹Department of Genetics, University of Georgia, Athens, GA, USA

30 ¹²The Center for Bioenergy Innovation, Oak Ridge National Laboratory, Oak Ridge, TN,
31 USA

32

33 ***CORRESPONDING AUTHORS:** Robert J. Schmitz, schmitz@uga.edu and Frank
34 Johannes, frank@johanneslab.org

35

36 **KEYWORDS:** Mutation rate, epimutation rate, epigenetics, poplar, DNA methylation

37

38 **ABSTRACT**

39

40 **Background:** Plants can transmit somatic mutations and epimutations to offspring,
41 which in turn can affect fitness. Knowledge of the rate at which these variations arise is
42 necessary to understand how plant development contributes to local adaption in an eco-
43 evolutionary context, particularly in long-lived perennials.

44 **Results:** Here, we generated a new high-quality reference genome from the oldest
45 branch of a wild *Populus trichocarpa* tree with two dominant stems which have been
46 evolving independently for 330 years. By sampling multiple, age-estimated branches of

47 this tree, we used a multi-omics approach to quantify age-related somatic changes at
48 the genetic, epigenetic and transcriptional level. We show that the per-year somatic
49 mutation and epimutation rates are lower than in annuals and that transcriptional
50 variation is mainly independent of age divergence and cytosine methylation.

51 Furthermore, a detailed analysis of the somatic epimutation spectrum indicates that
52 transgenerationally heritable epimutations originate mainly from DNA methylation
53 maintenance errors during mitotic rather than during meiotic cell divisions.

54 **Conclusion:** Taken together, our study provides unprecedented insights into the origin
55 of nucleotide and functional variation in a long-lived perennial plant.

56

57 **BACKGROUND**

58

59 The significance of somatic mutations, i.e., variations in DNA sequence that occur after
60 fertilization, in long-lived plant and animal species have been a point of debate and
61 investigation for the past 30 years [1–4]. It has been hypothesized that the evolutionary
62 consequences of such mutations are likely even more profound in woody perennial
63 plants, where undifferentiated meristematic cells produce all above-ground and below-
64 ground structures. As meristems undergo constant cell division throughout the lifetime
65 of a plant, somatic mutations arising in meristems may result in genetic differences
66 being passed onto progeny cells [5–8]. The accumulation of somatic mutations can thus
67 lead to genetic and occasionally also phenotypic divergence among vegetative lineages
68 within the same individual. In trees, for instance, different branches have been shown to
69 differ in their responses to pest and pathogen attack, alternate reactions to drought

70 and/or nutrient availability, or dissimilar demands for photosynthate material, even
71 within the same individual [9]. Beyond the impact of point mutations and small
72 insertions/deletions on gene function, alterations in chromatin structure and DNA
73 methylation might also impact gene expression variation.

74

75 Phenotypic variation has been attributed to somatic mutations in several perennial
76 plants, including the derivation of Nectarines in peach [10] and the origin of modern
77 grape cultivars (*Vitis vinifera* L.) [11]. In *Populus tremuloides*, somatic mutations have
78 been hypothesized as the cause for variation in DNA markers among individual ramets
79 of a single genotype [12]. Initial attempts to demonstrate within-tree mosaicism using
80 genetic markers [13], showed at low-resolution that the degree of intra-tree variability
81 was positively correlated with the physical distance between sampled branches. More
82 recently, work in oak (*Quercus rubur*) has documented variation in DNA sequence
83 among an independent sampling of alternate branches from a single genotype [14, 15].
84 They estimated a fixed mutation rate of $4.2 - 5.2 \times 10^{-8}$ substitutions per locus per
85 generation, which is only within one order of magnitude of the rate observed in the
86 herbaceous annual plant *Arabidopsis thaliana* [16]. These results are consistent with an
87 emerging hypothesis that the per-unit-time mutation rate of perennials is much lower
88 than in annuals to delay mutational meltdown [17, 18] and this lower rate is
89 accomplished by limiting the number of cell divisions between the meristem and the
90 new branch [19]. Additional recent studies have also revealed similar rates of
91 spontaneous mutations in a range of species including perennials [18]. Regardless of
92 the rate of mutation, the frequency of deleterious mutations in woody plants is high,

93 which is hypothesized to reduce survival of progeny resulting from inbreeding and favor
94 outcrossing as is observed in many forest trees [20, 21].

95

96 Similar to genetic mutations, phenotypic variation can be caused by epigenetic variation
97 such as stable changes in cytosine methylation or epimutations [22]. Cytosine
98 methylation is a covalent base modification that is inherited through both mitotic and
99 meiotic cell divisions in plants [23]. It occurs in three sequence contexts, CG, CHG, and
100 CHH (H = A, T, or C) and the pattern and distribution of methylation at these different
101 contexts is predictive of its function in genome regulation [24]. Spontaneous changes in
102 methylation independent of genetic changes can lead to phenotypic changes [25]. Well-
103 characterized examples in plants include the peloric phenotype in toadflax (*Linaria*
104 *vulgaris*), the colorless non-ripening phenotype in tomato (*Solanum lycopersicum*), and
105 the mantled phenotype in oil palm (*Elaeis guineensis*) [26–28].

106

107 Once established, epimutations can stably persist or be inherited across generations.
108 For example, the reversion rate from the colorless non-ripening epimutant allele to wild
109 type is about 1 in 1000 per generation in tomato [27]. Studies in *A. thaliana* mutation
110 accumulation lines have documented that the vast majority (91-99.998%) of methylated
111 regions in the genome are stably inherited across generations; only a small subset of
112 the methylome shows variation among mutation accumulation lines [29–31]. Estimates
113 in *A. thaliana* indicate that the spontaneous methylation gain and loss rates at CG sites
114 are 2.56×10^{-4} and 6.30×10^{-4} per generation per haploid methylome, respectively [32].
115 Despite the wealth of knowledge about transgenerational methylation inheritance, very

116 little is known about somatic epimutations, especially in long-lived perennial species.
117 Previous studies have been limited by resolution and time. Heer *et al.* observed no
118 global methylation changes and no consistent variation in gene body methylation
119 associated with growth conditions of Norway spruce [33]. Several studies have linked
120 stress conditions to differential methylation in perennials but did not look at the stability
121 of methylation after removing the stressor [34, 35]. One exception, Le Gac *et al.*,
122 identified environment-related differentially methylated regions in poplar, but only
123 examined stability across six months [36].

124
125 Detailed insights into the rate and spectrum of somatic mutations and epimutations are
126 necessary to understand how somatic development of long-lived perennials contribute
127 to population-level variation in an eco-evolutionary context. Here we generated a new
128 high-quality reference genome from the oldest branch of a wild *Populus trichocarpa* tree
129 with two dominant stems which have been evolving independently for approximately
130 330 years. By sampling multiple, age-estimated branches of this tree, we used a multi-
131 omics approach to quantify age-related somatic changes at the genetic, epigenetic and
132 transcriptional level. Our study provides the first quantitative insights into how nucleotide
133 and functional variation arise during the lifetime of a long-lived perennial plant.

134

135 **RESULTS**

136

137 **Experimental design for the discovery of somatic genetic and epigenetic variants**

138

139 A stand of trees was identified near Mount Hood, Oregon and vegetative samples were
140 collected from over 15 trees as part of an independent study. Of these trees, five were
141 chosen for subsequent analysis and five branches of each tree were identified (Fig. S1).
142 For each branch, the stem age was determined by coring the main stem at breast
143 height and where the branch meets the stem and the branch age was determined by
144 coring the base of the branch (Fig.1 and Fig. S2). Although 25 branches in total were
145 initially sampled, six were excluded from analysis because they were epicormic and age
146 estimates could not be determined. Two other branches had incomplete cores, but ages
147 could be estimated based on radial diameter.

148

149 From this, we were specifically interested in tree 13 and tree 14 (Fig. 1). Originally
150 identified as two separate genotypes, they are actually two main stems of a single basal
151 root system and trunk. Both tree 13 and tree 14 originated as stump sprouts off of an
152 older tree that was knocked down over 300 years ago. Attempts to determine the total
153 age were unsuccessful. However, statistical estimates based on molecular-clock
154 arguments and a regression analysis of diameter to age suggest that the tree is
155 approximately 330 years old (Shayary et al. 2019, co-submission).

156

157 Leaf samples were collected from eight age-estimated branches for multi-omics
158 analysis for tree 13 and tree 14. The oldest branch of tree 14 (branch 14.5) was used
159 for genome assembly of *Populus trichocarpa* var. *Stettler*. Genome resequencing was
160 performed for all branches to explore intra- and inter-tree genetic variation. PacBio,

161 MethylC-seq, and mRNA-seq libraries were constructed for the branches of tree 13 and
162 tree 14 to explore structural, methylation, and transcriptional variation, respectively.

163

164 **Genome assembly and annotation of *Populus trichocarpa* var. *Stettler***

165 We sequenced the *P. trichocarpa* var. *Stettler* using a whole-genome shotgun
166 sequencing strategy and standard sequencing protocols. Sequencing reads were
167 collected using Illumina and PacBio. The current release is based on PacBio reads
168 (average read length of 10,477 bp, average depth of 118.58x) assembled using the
169 MECAT CANU v.1.4 assembler [37] and subsequently polished using QUIVER [38]. A
170 set of 64,840 unique, non-repetitive, non-overlapping 1.0 kb sequences were identified
171 in the version 4.0 *P. trichocarpa* var. *Nisqually* assembly and were used to assemble
172 the chromosomes. The version 1 *Stettler* release contains 392.3 Mb of sequence with a
173 contig N50 of 7.5 Mb and 99.8% of the assembled sequence captured in the
174 chromosomes. Additionally, ~232.2 Mb of alternative haplotypes were identified.
175 Completeness of the final assembly was assessed using 35,172 annotated genes from
176 the version 4.0 *P. trichocarpa* var. *Nisqually* release (jgi.doe.gov). A total of 34,327
177 (97.72%) aligned to the primary *Stettler* assembly.

178 The annotation was performed using ~1.4 billion pairs of 2x150 stranded paired-end
179 Illumina RNA-seq GeneAtlas *P. trichocarpa* var. *Nisqually* reads, ~1.2 billion pairs of
180 2x100 paired-end Illumina RNA-seq *P. trichocarpa* var. *Nisqually* reads from Dr. Pankaj
181 Jaiswal, and ~430 million pairs of 2x75 stranded paired-end Illumina var. *Stettler* reads
182 using PERTRAN (Shu, unpublished) on the *P. trichocarpa* var. *Stettler* genome. About
183 ~3 million PacBio Iso-Seq circular consensus sequences were corrected and collapsed

184 by a genome-guided correction pipeline (Shu, unpublished) on the *P. trichocarpa* var.
185 *Stettler* genome to obtain ~0.5 million putative full-length transcripts. We annotated
186 34,700 protein-coding genes and 17,314 alternative splices for the final annotation.
187 Because of the extensive resources included in the annotation, 32,330 genes had full-
188 length transcript support.

189 **Identification and rate of somatic genetic variants**

190 Leaf samples from the five trees were sequenced to an average depth of ~87x (~60-
191 164x) using Illumina HiSeq. Roughly 88% of the high-quality reads map to the genome
192 and about 98.6% of the genome is covered by at least one read, and genome coverage
193 (~8-500x) used for SNP calling was about 97%. The initial number of SNPs per tree
194 (mutation on any branch) varied between 44,000 and 152,000, which is populated with
195 many false positives due to coverage, sequencing and alignment errors, etc. Applying
196 an additional filter requiring >20x coverage per position and requiring coverage in all
197 branches reduced the total amount genome space queried to ~40 Mb. Furthermore,
198 since most of the genome (99.9%) is homozygous at every base pair, a somatic
199 mutation will almost always result in a change from a homozygous to heterozygous site.
200 Restricting the analysis to sites that change from homozygous to heterozygous, we
201 identified 118 high-confidence SNPs in tree 13 and 143 high-confidence SNPs in tree
202 14 (Tables S1-2).

203 Over two-thirds of the SNPs in tree 13 and tree 14 were transition mutations, with C-G
204 to T-A mutations accounting for over 54% of the SNPs (Fig. 2a). Of the transversion
205 mutations C-G to G-C was the least common (3.8%) whereas C-G to A-T was most

206 common (10%). Nearly half of the SNPs (46%) occurred in transposable elements and
207 about 10% occur in promoter regions (Fig. 2b and Tables S1-S2). SNPs are significantly
208 enriched in TEs and depleted in promoter regions genome-wide (Chi-square, $df = 3$, $P <$
209 0.001)

210 To obtain an estimate of the rate of somatic point mutations from these SNP calls, we
211 developed *mutSOMA* (<https://github.com/jlab-code/mutSOMA>), a phylogeny-based
212 inference method that fully incorporates knowledge of the age-dated branching topology
213 of the tree (see Methods and Supplementary Text). Using this approach, we find that
214 the somatic point mutation rate in poplar is 1.33×10^{-10} (95% CI: $1.53 \times 10^{-11} - 4.18 \times 10^{-$
215 10) per base per haploid genome per year (Table S3). Generation time can refer to two
216 measurements—time from seed to production of first seeds and the organism’s lifespan.
217 In annual plants, these values can be considered the same; however, this is not the
218 case for perennials. Assuming 15 years from seed to production of first seeds [39], the
219 poplar seed-to-seed generation mutation rate would be approximately 1.99×10^{-9} . This
220 is slightly lower than the per-generation (seed-to-seed) mutation rate observed in the
221 annual *A. thaliana* (7×10^{-9}) [16]. Next looking at the lifespan per-generation rate and
222 assuming a maximum age of 200 years [40], the lifespan per-generation rate is $2.66 \times$
223 10^{-8} . This estimate is slightly lower than the per-generation somatic mutation rate
224 recently reported in oak ($4.2 - 5.8 \times 10^{-8}$) [14].

225

226 To analyze structural variants (SV) between haplotypes and somatic SV mutations,
227 PacBio libraries were generated for the eight branches from tree 13 and tree 14 (Fig. 1).
228 For each branch, four PacBio cells were sequenced generating an average output of

229 3.05 million reads and 28.3 Gb per branch (Table S4). After aligning the PacBio output
230 to the *P. trichocarpa* var. *Stettler* genome, calling SVs larger than 20 bp, and filtering,
231 we identified ~10,466 deletions, ~6,702 insertions, 645 duplications, and three
232 inversions between the reference *Stettler* haplotype and the alternative haplotype
233 (Table S5). Upon manual inspection of read mapping for a representative subset of
234 SVs, 72.6% of SVs have strong support where multiple aligned reads support the SV
235 type and size (Table S6). Deletions and duplications are significantly enriched in
236 tandem repeat sequence and depleted in genic sequence (Kolmogorov-Smirnov two-
237 sample test, P value $< 2.2 \times 10^{-16}$). Furthermore, deletions generally have less genic
238 sequence and more tandem repeat sequence than do duplications (Fig. S3). Several of
239 the detected SVs are large, with 11 deletions and five duplications greater than 50 kb
240 (Table S5) with genic sequence content ranging from 0.0% to 23.7%. Comparisons of
241 the branches from tree 13 and tree 14 did not identify instances of somatic SV mutation.

242

243 **Identification and rate of somatic epigenetic variants**

244

245 To explore somatic epigenetic variation associated with changes in DNA methylation,
246 we generated whole-genome bisulfite sequencing libraries from the branch tips of tree
247 13 and tree 14 (Fig. 1). The average genome coverage for the samples was ~41.1x and
248 sequence summary statistics are located in Table S7. Genome-wide methylation levels
249 were similar across all samples with 36.61% mCG, 19.02% mCHG, and 2.07% mCHH%
250 (Fig. S4) [41], indicating that global methylation levels are relatively stable across
251 branches. Nonetheless, we observed significant age-dependent DNA methylation

252 divergence between branches in CG and CHG contexts, both at the level of individual
253 cytosines as well as at the level of regions, i.e. clusters of cytosines (Fig. 3a-b, Fig. S5,
254 and Table S8). These age-dependent divergence patterns indicate that spontaneous
255 methylation changes (i.e. epimutations) are cumulative across somatic development
256 and thus point to a shared meristematic origin (Shahryary et al. 2019, co-submission).

257

258 To obtain an estimate of somatic epimutation rates, we applied *AlphaBeta* (Shahryary et
259 al. 2019, co-submission). The method builds on our previous approach for estimating
260 ‘germline’-epimutation in mutation accumulation (MA) lines [32], except here we treat
261 the tree branching topology as an intra-organismal phylogeny and model mitotic instead
262 of meiotic inheritance. Focusing first on cytosine-level epimutations, we estimated that
263 at the genome-wide scale spontaneous methylation gains in contexts CG and CHG
264 occur at a rate of 1.8×10^{-6} and 3.3×10^{-7} per site per haploid genome per year,
265 respectively; whereas spontaneous methylation losses in these two sequence contexts
266 occur at a rate of 5.8×10^{-6} and 4.1×10^{-6} per site per haploid genome per year. Based
267 on these estimates, we extrapolate that the *seed-to-seed* per-generation epimutation
268 rate in poplar is about 10^{-5} and the *lifespan* per-generation rate is 10^{-4} . Remarkably,
269 these estimates are very similar to those reported in *A. thaliana* MA lines [32]. The
270 observation that two species with such different life history traits and genome
271 architecture display very similar per-generation mutation and epimutation rates
272 suggests that the rates themselves are subject to strong evolutionary constraints.

273

274 In addition to global epimutation rates, we also estimated rates for different genomic
275 features (mRNA, promoters, intergenic, TEs). This analysis revealed highly significant
276 rate differences in the CG and CHG context between genomic features, with mRNAs
277 showing the highest and TEs the lowest combined rates (Fig. 3c-j). Interestingly, the
278 ordering of the magnitude of the mRNA, promoter, and intergenic rates is similar to that
279 previously observed in *A. thaliana* MA lines [32]. The differences in rates at local
280 genomic features likely reflect the distinct DNA methylation pathways that function on
281 these sequences (RNA-directed DNA methylation, CHROMOMETHYLASE3,
282 CHROMOMETHYLASE2, DNA METHYLTRANSFERASE1, etc.). For example, the high
283 rate of epimutation losses in mRNA relative to other features (Fig. 3g-h) could reflect the
284 activity of CMT3-mediated gene body DNA methylation [42, 43]. The observation that
285 the epimutation rates of these features is consistent between *A. thaliana* MA lines (>60
286 generations) and this long-lived perennial (within a single generation) seems to imply
287 that epimutations are not a result of biased reinforcement of DNA methylation during
288 sexual reproduction or environment/genetic variation, but instead a feature of DNA
289 methylation maintenance through mitotic cell divisions.

290

291 **Assessment of spontaneous differentially methylated regions**

292

293 Differentially methylated regions are functionally more relevant than individual cytosine-
294 level changes, as in certain cases they are linked to differential gene expression and
295 phenotypic variation [26–28, 44, 45]. To explore the extent of differentially methylated
296 regions (DMRs) that spontaneously arise in these trees we searched for all pairwise

297 DMRs between all branches. In total, we identified 10,909 DMRs that possessed
298 changes in all sequence contexts (CG, CHG and CHH - C-DMRs). Together they
299 constitute approximately 1.69 Mb of the total 167.4 Mb (~1%) of methylated sequences
300 in the *Stettler* genome and they reveal age-dependent accumulation (Fig. 4a). Most
301 DMRs occur in intergenic regions (56.7%), but a significant enrichment of DMRs were
302 detected within two kilobases from the transcriptional start site of genes compared to
303 methylated regions as a whole (Fig. 4b) (Fisher's exact test, one-sided, P value <
304 0.001).

305 Given the heterozygous nature of wild *P. trichocarpa*, we explored allelic methylation
306 changes. After filtering for sufficient coverage and methylation change, we assigned the
307 pseudo-allele state of each branch at 4,488 DMRs. Possible states were homozygous
308 unmethylated, heterozygous, and homozygous methylated. In each sample, 43.0% of
309 DMRs, on average, were categorized as homozygous methylated (Fig. S6).

310 Interestingly, the youngest branches, 13.1 and 14.1 have about 10% more homozygous
311 methylated pseudo-alleles than the other branches (51.1% vs 41.7%). Next, we looked
312 at the number of changes of pseudo-allele states. This is expected as DMRs were
313 identified as having different methylation levels in the samples. On average, there are
314 3.02 state changes for each DMR with 94.4% of DMRs having one to five state changes
315 (Fig. 4c). These data suggest that many of these regions are metastable, a common
316 feature of epimutations in plants.

317

318 An example of a region with one state change are the tree specific DMRs (Fig. 4d). In
319 these regions, all branches of one tree are homozygous unmethylated and all branches

320 of the other tree are homozygous methylated. This suggesting the methylation state
321 change occurred shortly after the trees separated and remained stable throughout
322 subsequent mitotic divisions. In contrast, we also identified highly variable regions with
323 seven state changes, a change between each branch (Fig. 4e). Of the regions with two
324 state changes, 150 have branch-specific state changes. For example, in Fig. 4f
325 branches 13.1 to 13.3 are homozygous unmethylated, then it changes to homozygous
326 methylated for branch 13.5, and changes again to homozygous unmethylated for
327 branches 14.5 – 14.2. Similarly, in Fig. 4g, all branches except 14.5 are homozygous
328 methylated and 14.5 has spontaneously lost methylation.

329

330 We also used the identified C-DMRs (differential methylation in all cytosine sequence
331 contexts) to obtain region-level epimutation rates. To do this, we established control
332 regions ('non-DMR') with the same size distribution as observed for C-DMRs and used
333 the methylation levels of all cytosines in each (non-)DMR to calculate methylation levels
334 per region. Interestingly, this analysis shows that region-level epimutation rates are
335 comparable to epimutation rates of single cytosines. Even though there are far fewer
336 DMRs in comparison to epimutations at single cytosines, the similar rates are not too
337 unexpected if one considers that the total 'epimutable space' for regions in the genome
338 is much smaller than that for individual cytosines. In summary, these results might
339 suggest that the mechanisms which underlie spontaneous differential methylation are
340 the same for differential methylation in larger regions and at individual sites.

341

342 **Functional consequences of differential methylation on gene expression**

343

344 To assess if age-related cytosine methylation changes have functional consequences,
345 we performed mRNA-seq with three biological replicates for each branch of trees 13
346 and 14. On average, each library had over ~55 million reads and 96.8% mapping to the
347 *P. trichocarpa* var. *Stettler* genome (Table S9). We used DESeq2 to identify
348 differentially expressed genes (DEGs) pairwise between branches [46] and identified a
349 total of 2,937 genes. The *P. trichocarpa* var. *Stettler* genome has 34,700 annotated
350 genes, so this differential expression gene set is 8.46% of all genes and 10.5% of
351 expressed genes.

352

353 Since the somatic accumulation of spontaneous methylation changes could affect gene
354 expression, we asked if transcriptional divergence also increases as a function of tree
355 age. We found that in contrast to somatic mutations and epimutations, the divergence
356 between leaf transcriptomes is much more heterogeneous and displays only a weak
357 and non-significant accumulation trend (Fig. 5a). This observation suggests that the
358 accumulation of genetic and epigenetic changes are largely uncoupled from age-
359 dependent transcriptional changes in poplar, at least at the global scale.

360

361 However, this global analysis does not rule out that DNA methylation changes at
362 specific individual loci can have transcriptional consequences. To explore this in more
363 detail, we analyzed DMRs proximal to DEGs, and correlated the methylation level of the
364 DMR with the expression level of the gene. The correlation is positive when a higher
365 methylation level in the DMR is associated with higher expression of the gene.

366 Regardless of where the DMR was located relative to the gene, we observed positive
367 DMR-DEG correlations and negative DMR-DEG correlations. There was no bias for
368 direction of correlation and genomic feature type (Fig. 5b).

369

370 We further focused on four specific examples where DEG-DMR correlations were
371 statistically significant (Fig. S7). Of these four, three of the DMRs occurred within two
372 kilobases upstream of the transcription start site, and they have strong negative
373 correlations (Fig. 5c). The DMR located in the untranslated region of a gene encoding a
374 mitochondrial oxoglutarate/malate carrier protein was positively correlated with gene
375 expression (Fig. 5d), although it remains unclear if this relationship is causal.

376

377 Taken together, our transcriptome analysis indicates that gene expression changes in
378 this poplar tree are largely independent of methylation at both the global and local scale
379 except for a few rare examples. This observation is at least partly consistent with our
380 model-based analyses, which suggest that somatic epimutations in this tree accumulate
381 neutrally (Shahryary et al. 2019, co-submission).

382

383 **DISCUSSION**

384

385 Using a multi-omics approach, we were able to calculate the rates of somatic mutations
386 and epimutations in the long-lived perennial tree *P. trichocarpa*. Consistent with the per-
387 unit-time hypothesis, we find that the per-year genetic and epigenetic mutation rates in
388 poplar are lower than in *A. thaliana*, which is remarkable considering that the former

389 experienced hundreds of years of variable environmental conditions. This observation
390 supports the view that long-lived perennials may limit the number of meristematic cell
391 divisions during their lifetime and that they have evolved mechanisms to protect these
392 cell types from the persistent influence of environmental mutagens, such as UV-
393 radiation. Interestingly, in contrast to the observed differences in *per-year* mutation and
394 epimutation rates, our analysis reveals strong similarities in the *per-generation* rates
395 between these two species. This close similarity further suggests that the per-
396 generation rates of spontaneous genetic and epigenetic changes are under strong
397 evolution constraint, although it remains unclear from our experimental design how
398 many of these (epi)mutations will be successfully transferred to the next generation.

399

400 The results presented here are most certainly an underestimate of the actual rate. This
401 may be a result of the sampling biased used in this study, as we were only able to
402 sample surviving branches and identify mutations that occurred early enough that they
403 are present in the majority of the cells sampled in the tissues profiled. Perhaps variable
404 environmental conditions lower the epimutation rate by keeping the cells in sync, thus
405 few differences can be observed. Alternatively, meristematic cells that give rise to the
406 sampled tissues have highly reinforced and well-maintained DNA methylomes similar to
407 observations in embryonic tissue [47–51]. Either scenario would imply that most of the
408 identified epimutations are spontaneous in nature. Although the rate is different, the
409 ordering in feature-specific epimutation rates is the same between poplar and *A.*
410 *thaliana*, suggesting that this is a general pattern in plant genomes, which likely is
411 derived from maintenance of DNA methylation through mitotic cell divisions.

412

413 **CONCLUSION**

414

415 Taken together, our study provides unprecedented insights into the origin of nucleotide,
416 epigenetic, and functional variation in the long-lived perennial plant.

417

418

419 **METHODS**

420

421 **Sample collection and age estimation**

422

423 The trees used in this study were located at Hood River Ranger District [Horse Thief
424 Meadows area], Mt. Hood National Forest, 0.6 mi south of Nottingham Campground off
425 OR-35 at unmarked parking area, 500' west of East Fork Trail #650 across river, ca.
426 45.355313, -121.574284 (Fig. S1).

427

428 Cores were originally collected from the main stem and five branches from each of five
429 trees in April 2015 at breast height (~1.5 m) for standing tree age using a stainless-steel
430 increment borer (5 mm in diameter and up to 28 cm in length). Cores were mounted on
431 grooved wood trim, dried at room temperature, sanded and stained with 1%
432 phloroglucinol following the manufacturer's instructions ([https://www.forestry-
433 suppliers.com/Documents/1568_msds.pdf](https://www.forestry-suppliers.com/Documents/1568_msds.pdf)). Annual growth rings were counted to
434 estimate age. For cores for which accurate estimates could not be made from the 2015

435 collection, additional collections were made in spring 2016. However, due to difficulty in
436 collecting by climbing, many of the cores did not reach the center of the stem or
437 branches (pith) and/or the samples suffered from heart rot. Combined with the difficulty
438 in demarcating rings in porous woods such as poplar *Populus* [52, 53], accurate
439 measures of tree age or branch age were challenging (Fig. S2).

440

441 Simultaneously with stem coring, leaf samples were collected from the tips of each of
442 the branches from the selected five trees. Branches 9.1, 9.5, 13.4, 14.1, 15.1, and 15.5
443 were too damaged to determine reasonable age estimates and were removed from
444 analysis. Branch 14.4 and the stems of 13.1 and 13.2 were estimated by simply
445 regressing the diameter of all branches and stems that could be aged by coring.

446

447 **Nuclei prep for DNA extraction**

448

449 Poplar leaves, that had been kept frozen at -80 °C, were gently ground with liquid
450 nitrogen and incubated with NIB buffer (10 mM Tris-HCL, PH8.0, 10 mM EDTA PH8.0,
451 100 mM KCL, 0.5 M sucrose, 4 mM spermidine, 1 mM spermine) on ice for 15 min.
452 After filtration through miracloth, Triton x-100 (Sigma) was added to tubes at a 1:20
453 ratio, placed on ice for 15 min, and centrifuged to collect nuclei. Nuclei were washed
454 with NIB buffer (containing Triton x-100) and re-suspended in a small amount of NIB
455 buffer (containing Triton x-100) then the volume of each tube was brought to 40 ml and
456 centrifuged again. After careful removal of all liquid, 10 ml of Qiagen G2 buffer was
457 added followed by gentle re-suspension of nuclei; then 30 ml G2 buffer with RNase A

458 (to final concentration of 50 mg/ml) was added. Tubes were incubated at 37 °C for 30
459 min. Proteinase K (Invitrogen), 30 mg, was added and tubes were incubated at 50 °C
460 for 2 h followed by centrifugation for 15 min at 8000 rpm, at 4 °C, and the liquid gently
461 poured to a new tube. After gentle extraction with Chloroform / isoamyl alcohol (24:1),
462 then centrifugation and transfer of the top phase to a fresh tube, HMW DNA was
463 precipitated by addition of 2/3 volume of iso-propanol and re-centrifugation to collect the
464 DNA. After DNA was washed with 70% ethanol, it was air dried for 20 min and dissolved
465 thoroughly in 1x TE.

466

467 **Whole-genome sequencing**

468

469 We sequenced *Populus trichocarpa* var. *Stettler* using a whole-genome shotgun
470 sequencing strategy and standard sequencing protocols. Sequencing reads were
471 collected using Illumina and PacBio. Both the Illumina and PacBio reads were
472 sequenced at the Department of Energy (DOE) Joint Genome Institute (JGI) in Walnut
473 Creek, California and the HudsonAlpha Institute in Huntsville, Alabama. Illumina reads
474 were sequenced using the Illumina HiSeq platform, while the PacBio reads were
475 sequenced using the RS platform. One 400-bp insert 2x150 Illumina fragment library
476 was obtained for a total of ~349x coverage (Table S10). Prior to assembly, all Illumina
477 reads were screened for mitochondria, chloroplast, and phix contamination. Reads
478 composed of >95% simple sequence were removed. Illumina reads less than 75 bp
479 after trimming for adapter and quality (q < 20) were removed. The final Illumina read set
480 consists of 906,280,916 reads for a total of ~349x of high-quality Illumina bases. For the

481 PacBio sequencing, a total of 69 chips (P6C4 chemistry) were sequenced with a total
482 yield of 59.29 Gb (118.58x) with 56.2 Gb > 5 kb (Table S11), and post error correction a
483 total of 37.3 Gb (53.4x) was used in the assembly.

484

485 **Genome assembly and construction of pseudomolecule chromosomes**

486

487 The current release is version 1.0 release began by assembling the 37.3 Gb corrected
488 PacBio reads (53.4x sequence coverage) using the MECAT CANU v.1.4 assembler [37]
489 and subsequently polished using QUIVER v.2.3.3 [38]. This produced 3,693 scaffolds
490 (3,693 contigs), with a scaffold N50 of 1.9 Mb, 955 scaffolds larger than 100 kb, and a
491 total genome size of 693.8 Mb (Table S12). Alternative haplotypes were identified in the
492 initial assembly using an in-house Python pipeline, resulting in 2,972 contigs (232.3 Mb)
493 being labeled as alternative haplotypes, leaving 745 contigs (461.5 Mb) in the single
494 haplotype assembly. A set of 64,840 unique, non-repetitive, non-overlapping 1.0 kb
495 syntenic sequences from version 4.0 *P. trichocarpa* var. *Nisqually* assembly and aligned
496 to the MECAT CANU v.1.4 assembly and used to identify misjoins in the *P. trichocarpa*
497 var. *Stettler* assembly. A total of 22 misjoins were identified and broken. Scaffolds were
498 then oriented, ordered, and joined together into 19 chromosomes. A total of 117 joins
499 were made during this process, and the chromosome joins were padded with 10,000
500 Ns. Small adjacent alternative haplotypes were identified on the joined contig set.
501 Althap regions were collapsed using the longest common substring between the two
502 haplotypes. A total of 14 adjacent alternative haplotypes were collapsed.

503

504 The resulting assembly was then screened for contamination. Homozygous single
505 nucleotide polymorphisms (SNPs) and insertion/deletions (InDels) were corrected in the
506 release sequence using ~100x of Illumina reads (2x150, 400-bp insert) by aligning the
507 reads using bwa-0.7.17 mem [54] and identifying homozygous SNPs and InDels with
508 the GATK v3.6's UnifiedGenotyper tool [55]. A total of 206 homozygous SNPs and
509 11,220 homozygous InDels were corrected in the release. Heterozygous SNP/indel
510 phasing errors were corrected in the consensus using the 118.58x raw PacBio data. A
511 total of 66,124 (1.98%) of the heterozygous SNP/InDels were corrected. The final
512 version 1.0 improved release contains 391.2 Mb of sequence, consisting of 25 scaffolds
513 (128 contigs) with a contig N50 of 7.5 Mb and a total of 99.8% of assembled bases in
514 chromosomes. Plots of the *Nisqually* marker placements for the 19 chromosomes are
515 shown in Fig. S8.

516

517 **Genome annotation**

518

519 Transcript assemblies were made from ~1.4 billion pairs of 2x150 stranded paired-end
520 Illumina RNA-seq GeneAtlas *P. trichocarpa* Nisqually reads, ~1.2 billion pairs of 2x100
521 paired-end Illumina RNA-seq *P. trichocarpa* Nisqually reads from Dr. Pankaj Jaiswal,
522 and ~430M pairs of 2x75 stranded paired-end Illumina var. *Stettler* reads using
523 PERTRAN (Shu, unpublished) on *P. trichocarpa* var. *Stettler* genome. About ~3M
524 PacBio Iso-Seq circular consensus sequences were corrected and collapsed by
525 genome guided correction pipeline (Shu, unpublished) on *P. trichocarpa* var. *Stettler*
526 genome to obtain ~0.5 million putative full-length transcripts. 293,637 transcript

527 assemblies were constructed using PASA [56] from RNA-seq transcript assemblies
528 above. Loci were determined by transcript assembly alignments and/or EXONERATE
529 alignments of proteins from *A. thaliana*, soybean, peach, Kitaake rice, *Setaria viridis*,
530 tomato, cassava, grape and Swiss-Prot proteomes to repeat-soft-masked *P. trichocarpa*
531 var. *Stettler* genome using RepeatMasker [57] with up to 2-kb extension on both ends
532 unless extending into another locus on the same strand. Gene models were predicted
533 by homology-based predictors, FGENESH+[58], FGENESH_EST (similar to
534 FGENESH+, EST as splice site and intron input instead of protein/translated ORF), and
535 EXONERATE [59], PASA assembly ORFs (in-house homology constrained ORF finder)
536 and from AUGUSTUS via BRAKER1 [60]. The best scored predictions for each locus
537 are selected using multiple positive factors including EST and protein support, and one
538 negative factor: overlap with repeats. The selected gene predictions were improved by
539 PASA. Improvement includes adding UTRs, splicing correction, and adding alternative
540 transcripts. PASA-improved gene model proteins were subject to protein homology
541 analysis to above mentioned proteomes to obtain Cscore and protein coverage. Cscore
542 is a protein BLASTP score ratio to MBH (mutual best hit) BLASTP score and protein
543 coverage is highest percentage of protein aligned to the best of homologs. PASA-
544 improved transcripts were selected based on Cscore, protein coverage, EST coverage,
545 and its CDS overlapping with repeats. The transcripts were selected if its Cscore is
546 larger than or equal to 0.5 and protein coverage larger than or equal to 0.5, or it has
547 EST coverage, but its CDS overlapping with repeats is less than 20%. For gene models
548 whose CDS overlaps with repeats for more that 20%, its Cscore must be at least 0.9
549 and homology coverage at least 70% to be selected. The selected gene models were

550 subject to Pfam analysis and gene models whose protein is more than 30% in Pfam TE
551 domains were removed and weak gene models. Incomplete gene models, low
552 homology supported without fully transcriptome supported gene models and short single
553 exon (< 300-bp CDS) without protein domain nor good expression gene models were
554 manually filtered out.

555

556 **SNP calling methods**

557

558 Illumina HiSeq2500 paired-end (2×150) reads were mapped to the reference genome
559 using bwa-mem [54]. Picard toolkit was used to sort and index the bam files. GATK [55]
560 was used further to align regions around InDels. Samtools v1.9 [61] was used to create
561 a multi-sample pileup for each tree independently. Preliminary SNPs were called using
562 VarScan v2.4.0 [62] with a minimum coverage of 21.

563

564 At these SNPs, for each branch, we calculated the conditional probability of each
565 potential genotype (RR, RA, AA) given the read counts of each allele, following SeqEM
566 [63], using an estimated sequencing error rate of 0.01. We identified high-confidence
567 genotype calls as those with a conditional probability 10,000x greater than the
568 probabilities of the other possible genotypes. We identified potential somatic SNPs as
569 those with both a high-confidence homozygous and high-confidence heterozygous
570 genotype across the branches.

571

572 We notice that the default SNP calling parameters tend to overcall homozygous-
573 reference allele genotypes and that differences in sequencing depth can bias the
574 relative number of heterozygous SNPs detected. To overcome these issues, we re-
575 called genotypes using conditional probabilities using down sampled allele counts. To
576 do this, we first randomly selected a set number of sequencing reads for each library at
577 each potential somatic SNP so that all libraries have the same sequencing depth at all
578 SNPs. Using the down sampled reads, we calculate the relative conditional probability
579 of each genotypes by dividing the conditional probabilities by the sum of the conditional
580 probabilities of all three potential genotypes. These relative probabilities are then
581 multiplied by the dosage assigned to their respective genotype (0 for RR, 1 for RA, 2 for
582 AA), and the dosage genotype is the sum of these values across all 3 possible
583 genotypes. Discrete genotypes were assigned using the following dosage values: RR =
584 dosage < 0.1; RA = 0.9 < dosage < 1.1; AA = dosage > 1.9. Dosages outside those
585 ranges are assigned a NA discrete genotype. SNPs with an NA discrete genotype or
586 depth below the down sampling level in any branch of a tree were removed from further
587 analysis. We performed three replicates of this procedure for depths of 20, 25, 30, 35,
588 40, and 45 reads.

589

590 PacBio libraries for each branch were sequenced using the PacBio Sequel platform,
591 fastq files aligned to the *P. trichocarpa* var. Stettler14 reference genome using ngmlr
592 [64], and multi-sample mileup files generated using in Samtools v1.9 [61] to quantify the
593 allele counts at the potential somatic SNPs. We used a minimum per-sample sequence

594 depth of 20 reads and used an alternate-allele threshold of 0.1 to call a heterozygote
595 genotype in the PacBio data.

596

597 To identify high-confidence candidate somatic SNPs, we identified potential somatic
598 SNPs with the same genotypes across branches using both the Illumina-based PacBio-
599 based genotypes, only including SNPs with full data in all branches for both types of
600 genotypes. Of these, we only retained SNPs that are homozygous in a single branch or
601 have a single homozygous-to-heterozygous transition (and no reversion) going from the
602 lowest to highest branches.

603

604 **Estimating somatic nucleotide mutation rate**

605

606 Building on the analytical framework developed in van der Graaf et al. (2015) and
607 Shahryary et al. 2019 (co-submission), we developed *mutSOMA*
608 (<https://github.com/jlab-code/mutSOMA>), a statistical method for estimating genetic
609 mutation rates in long-lived perennials such as trees. The method treats the tree
610 branching structure as a pedigree of somatic lineages and uses the fact that these cell
611 lineages carry information about the mutational history of each branch. A detailed
612 mathematical description of the method is provided in Supplementary Text. But briefly,
613 starting from the .vcf* files from S samples representing different branches of the tree,
614 we let G_{ik} be the observed genotype at the k -th single nucleotide ($k = 1, \dots, N$) in the i -th
615 sample, where N is the effective genome size (i.e. the total number of bases with
616 sufficient coverage). With four possible nucleotides (A, C, T, G), G_{ik} can have 16

617 possible genotypes in a diploid genome, 4 homozygous (A|A, T|T, C|C, G|G) and 12
618 heterozygous (A|G, A|T, ..., G|C). Using this coding, we calculate the genetic
619 divergence, D , between any two samples i and j as follows:

620

$$621 \quad D_{ij} = \sum_{k=1}^N I(G_{ik}, G_{jk}) N^{-1},$$

622

623 where $I(G_{ik}, G_{jk})$ is an indicator function, such that, $I(G_{ik}, G_{jk}) = 1$ if the two samples
624 share no alleles at locus k , 0.5 if they share one, and 0 if they share both alleles. We
625 suppose that D_{ij} is related to the developmental divergence time of samples i and j
626 through a somatic mutation model M_{θ} . The divergence times can be calculated from the
627 coring data (Table S13). We model the genetic divergence using

628

$$629 \quad D_{ij} = c + D_{ij}^*(M_{\theta}) + \epsilon_{ij},$$

630

631 where $\epsilon_{ij} \sim N(0, \sigma^2)$ is the normally distributed residual, c is the intercept, and $D_{ij}^*(M_{\theta})$
632 is the expected divergence as a function of mutation model M with parameter vector Θ .
633 Parameter vector Θ contains the unknown mutation rate δ and the unknown proportion
634 γ heterozygote loci of the most recent common ‘founder’ cells of samples i and j . The
635 theoretical derivation of $D_{ij}^*(M_{\theta})$ and details regarding model estimation can be found in
636 Supplementary Text. The estimation of the residual variance in the model allows for the
637 fact that part of the observed genetic divergence between any two samples is driven

638 both by genotyping errors as well as by somatic genetic drift as meristematic cells pass
639 through bottlenecks in the generation of the lateral branches.

640

641 **Structural variant analysis methods**

642

643 For structural variant (SV) analysis, PacBio libraries were generated for four branches
644 from the tree 13 and four branches from tree 14 with four sequencing cells sequenced
645 per branch using the PacBio Sequel platform. PacBio fastq files were aligned to the *P.*
646 *trichocarpa* var. *Stettler* reference genome using ngmlr v.0.2.6 [64] using a value of 0.01
647 for the "-R" flag. SVs were discovered and called using pbsv (pbsv v2.2.0,
648 <https://github.com/PacificBiosciences/pbsv>). SV signatures were identified for each
649 sample using 'pbsv discover' using the '--tandem-repeats' flag and a tandem repeat
650 BED file generated using trf v4.09 [65] for the *P. trichocarpa* var. *Stettler* genome. SVs
651 were called jointly for all 8 branches using 'pbsv call'. The output from joint SV calling
652 changes slightly depending on the order of the samples used for the input in 'pbsv call',
653 so four sets of SVs were generated using four different sample orders as input. We
654 used a custom R script [66] to filter the SV output from pbsv. We remove low-complexity
655 insertions or deletions with sequence containing > 80% of a mononucleotide 8-mer,
656 50% of a single type of binucleotide 8-mer, or 60% of two types of binucleotide 8-
657 mers. We required a minimum distance of 1 kb between SVs. We removed SVs with
658 sequencing coverage of more than three standard deviations above the mean coverage
659 across a sample. After calling genotypes, any SVs with missing genotype data were
660 removed.

661

662 Genotypes were called based on the output from pbsv using a custom R script. We
663 required a minimum coverage of 10 reads in all sample and for one sample to have at
664 least 20 reads. We required a minimum penetrance (read ratio) of 0.25 and at least 2
665 reads containing the minor allele for a heterozygous genotype. We allowed a maximum
666 penetrance of 0.05 for homozygous genotypes. For each genotype, we assigned a
667 quality score based on the binomial distribution-related relative probability of the 3
668 genotype classes (RR, AR, AA) based on A:R read ratio, using an estimated
669 sequencing error of 0.032, and an estimated minimum allele penetrance of 0.35. For a
670 genotype with a score below 0.9 but with the same genotype at the SV as another
671 sample with a score above 0.98, the score was adjusted by multiplying by 1.67. Any
672 genotypes with adjusted scores below 0.9 were converted to NA. For deletions,
673 duplications, and insertions, 10 representatives in different size classes were randomly
674 selected and the mapping patterns of reads were visually inspected using IGV v2.5.3
675 [67] to assign scores indicating how well the visual mapping patterns support the SV
676 designation. Scores were defined by the following: “strong”, multiple reads align to the
677 same locations in the reference genome that support the SV type and size; “moderate”,
678 multiple reads align to the same reference location for one side of the SV but align to
679 different or multiple locations in the region for the other side of the SV; and “weak”,
680 reads align to reference locations that indicate a different SV type or much different SV
681 size.

682

683 The percent of genic sequence and tandem repeat sequence in deletions and
684 duplications were calculated using the *P. trichocarpa* var. *Stettler* annotation and
685 tandem repeat BED from above, respectively. Genome-wide expectations were derived
686 by separating the genome into 10-kb windows and calculating the percent genic and
687 tandem repeat sequence in each window. The distribution of genic and tandem repeat
688 sequences in deletions and duplications were compared to genome-wide expectations
689 using the Kolmogorov-Smirnov two-sample test (one-sided, $N_{\text{null}} = 39,151$, $N_{\text{del}} =$
690 $10,433$, $N_{\text{dup}} = 630$).

691
692 SVs showing variation between branches and identified in all 4 replicates are potential
693 instances of somatic SV mutations or loss-of-heterozygosity gene conversions, and the
694 mapping positions of sequencing reads were visually inspected with IGV [67] to confirm
695 the variation at these SVs.

696

697 **MethylC-seq sequencing and analysis**

698

699 A single MethylC-seq library was created for each branch from leaf tissue. Libraries
700 were prepared according to the protocol described in Urich *et al.* [68]. Libraries were
701 sequenced to 150-bp per read at the Georgia Genomics & Bioinformatics Core (GGBC)
702 on a NextSeq500 platform (Illumina). Average sequencing depth was ~41.1x among
703 samples (Table S7).

704

705 MethylC-seq reads were processed and aligned using Methylypy v1.3.2 [69]. Default
706 parameters were used expect for the following: clonal reads were removed, lambda
707 DNA was used as the unmethylated control, and binomial test was performed for all
708 cytosines with at least three mapped reads.

709

710 **Identification of Differentially Methylated Regions**

711

712 Identification of differentially methylated regions (DMRs) was performed using Methylypy
713 v1.3.2 [69]. All methylome samples were analyzed together to conduct an undirected
714 identification of DMRs across all samples in the CNN (N=A, C, G, T) context. Default
715 parameters were used. Only DMRs at least 40-bp long with at least three differentially
716 methylated cytosines (DMS) and five or more cytosines with at least one read were
717 retained. For each DMR, the weighted methylation level was computed as $mC / (mC +$
718 $uC)$ where mC and uC are the number of reads supporting a methylated cytosine and
719 unmethylated cytosine, respectively [41].

720

721 To identify epigenetic variants in these samples, we used a one-sided z-test to test for a
722 significant difference in methylation level of DMRs pairwise between branches. For each
723 pair, only DMRs with at least 5% difference in methylation level were used, regardless
724 of underlying context. Resulting P values were adjusted using Benjamini-Hochberg
725 correction ($N = 383,600$) with $FDR = 0.05$ [70] and DMRs are defined by adjusted P
726 value ≤ 0.05 .

727

728 **Identification of Methylated Regions**

729

730 For each sample, an unmethylated methylome was generated by setting the number of
731 methylated reads to zero while maintaining the total number of reads. Methylpy DMR
732 identification program [69] was applied to each sample using the original methylome
733 and unmethylated methylome with the same parameters as used for DMR identification.
734 Regions less than 40 bp-long, fewer than three DMS, and fewer than five cytosines with
735 at least one read were removed. Remaining regions from all samples were merged
736 using BEDtools v2.27.1 [71].

737

738 **Assigning genomic features to DMRs**

739

740 A genomic feature map was created such that each base pair of the genome was
741 assigned a single feature type (transposable element/repeat, promoter, untranslated
742 region, coding sequence, and intron) based on the previously described annotation.
743 Promoters were defined as 2 kb upstream of the transcription start site of protein-coding
744 genes. At positions where multiple feature types could be applicable, such as a
745 transposon in an intron or promoter overlapping with adjacent gene, priority was given
746 to untranslated regions (highest), introns, coding sequences, promoter, and transposon
747 (lowest). Positions without an assignment were considered intergenic. Genomic feature
748 content of each DMR and methylated region was assigned proportionally based on the
749 number of bases in each category.

750

751 **Identification of pseudo-allele methylation**

752

753 We aimed to categorize the DMRs into three pseudo-allele states: homozygous
754 methylated, heterozygous, and homozygous unmethylated. First, DMRs were filtered on
755 the following criteria: i) at least 25% change in weighted CG methylation level between
756 the highest and lowest methylation level of the samples; ii) at least one sample had a
757 CG methylation level of at least 75%; and iii) at least two “covered” CG positions. A
758 “covered” CG is defined as having at least one read for both symmetrical cytosines in all
759 samples. After filtering, 4,488 regions were used for analysis.

760

761 For each region in each sample, we next categorize the aligned reads overlapping the
762 region. If at least 35% of its “covered” CG sites are methylated, the read is categorized
763 as methylated. Otherwise it is an unmethylated read. Finally, we define the pseudo-
764 allele state by the portion of methylated reads; homozygous unmethylated: $\leq 25\%$,
765 heterozygous: $> 25\%$ and $< 75\%$, and homozygous methylated: $\geq 75\%$.

766

767 The null distribution was created by randomly shuffling the filtered DMRs in the genome
768 such that each simulated region is the same length as the original and it has at least two
769 “covered” CGs. The above procedure was applied and number of epigenotype changes
770 was determined. This was repeated for a total of 10 times.

771

772 The following special classes of DMRs were identified: highly variable, single loss,
773 single gain, and tree specific. A DMR is highly variable if there were pseudo-allele

774 changes between all adjacent branches. A DMR is single loss if all but one branch was
775 homozygous methylated, and one was homozygous unmethylated. Similarly, a DMR is
776 single gain if all but one branch was homozygous unmethylated and one branch was
777 homozygous methylated. Finally, a DMR is “tree specific” if all tree 13 branches were
778 homozygous unmethylated and all tree 14 branches were homozygous methylated or
779 vice versa.

780

781 **Estimating somatic epimutation rate**

782

783 We previously developed a method for estimating ‘germline’ epimutation rates in *A.*
784 *thaliana* based on multi-generational methylation data from Mutation Accumulation lines
785 [32]. In a companion method paper to the present study (Shahryary et al. 2019, co-
786 submission), we have extended this approach to estimating somatic epimutation rates in
787 long-lived perennials such as trees using leaf methylomes and coring data as input.
788 This new inference method, which we call *AlphaBeta*, treats the tree branching structure
789 as a pedigree of somatic lineages using the fact that these cell lineages carry
790 information about the epimutational history of each branch. *AlphaBeta* is implemented
791 as a bioconductor R package
792 (<http://bioconductor.org/packages/devel/bioc/html/AlphaBeta.html>). Using this approach,
793 we estimate somatic epimutation rates for individual CG, CHG, and CHH sites
794 independently, but also for regions. For the region-level analysis, we first use the
795 differentially methylated regions (DMRs) identified above. Sampling from the distribution
796 of DMR sizes, we then split the remainder of the genome into regions, which we refer to

797 as “non-DMRs”. Per sample, we aggregate the total number of methylated Cs and
798 unmethylated Cs in each region corresponding to a DMRs or a non-DMRs and used
799 these counts as input for *AlphaBeta*.

800

801 **mRNA-seq sequencing and analysis**

802

803 Total RNA was extracted from leaf tissue in each branch using the Direct-zol RNA
804 MiniPrep Plus kit (Zymo Research) with Invitrogen’s Plant RNA Reagent. Total RNA
805 quality and quantity were assessed before library construction. Strand-specific RNA-seq
806 libraries were constructed using the TruSeq Stranded mRNA LT kit (Illumina) following
807 the manufacturer’s instructions. For each sample, three independent libraries (technical
808 replicates) were constructed. Libraries were sequenced to paired-end 75-bp reads at
809 the GGBC on a NextSeq500 platform (Illumina). Summary statistics are included in the
810 Table S9.

811

812 For analysis, first, paired-end reads were trimmed using Trimmomatic v0.36 [72].
813 Trimming included removing TruSeq3 adapters, bases with quality score less than 10,
814 and any reads less than 50-bp long. Second, remaining reads were mapped to the
815 *Stettler* genome with HiSAT2 [73] using default parameters except to report alignments
816 for transcript assemblers (--dta). The HiSAT2 transcriptome index was created using
817 extracted splice sites and exons from the gene annotation as recommended. Last,
818 transcriptional abundances for genes in the reference annotation were computed for
819 each sample using StringTie v1.3.4d [74]. Default parameters were used except to limit

820 estimates to reference transcripts. TPM (transcripts per million) values were outputted
821 to represent transcriptional abundance.

822

823 **Identification of differentially expressed genes**

824

825 Differentially expressed genes (DEGs) were identified using DeSeq2 v1.22.2 [46]. The
826 count matrix was extracted from StringTie output files and the analysis was performed
827 using the protocol (ccb.jhu.edu/software/stringtie/index.shtml?t=manual#deseq).

828 Abundances for all samples were joined into one DESeq dataset with $\alpha = 0.01$. Gene
829 abundance was compared between all samples pairwise. In each pair, a gene was
830 considered differentially expressed if the adjusted P value ≤ 0.01 and the \log_2 -fold
831 change ≥ 1 . Genes differentially expressed in any pair were included for subsequent
832 analysis.

833

834 **Overlap of DMRs and DEGs**

835

836 We identified DMRs which overlapped the promoter region (2 kb upstream of
837 transcription start site) and gene body of annotated genes. For each DMR-gene pair, we
838 computed the Pearson's product moment correlation coefficient between the weighted
839 methylation level of the DMR and average gene abundance among replicates in TPM.
840 Next, looking only at genes which were previously identified as differentially expressed,
841 we performed a two-sided Pearson's correlation test for each DMR-DEG pair to test for
842 statistically significant correlations. Resulting P values were multiple test corrected with

843 Benjamini-Hochberg correction (N = 382, FDR = 0.05) [70]. Adjusted *P* values \leq 0.05
844 were considered significantly correlated.

845

846 **DECLARATIONS**

847

848 **Ethics approval and consent to participate**

849

850 Not applicable

851

852 **Consent for publication**

853

854 Not applicable

855

856 **Availability of data and materials**

857

858 Raw sequence data used for genome assembly, resequencing and identification of
859 structural variation of individual branches are available at NCBI SRA (PRJNA516415).

860 Raw sequence data for whole-genome bisulfite sequencing and mRNA-sequencing are
861 available in GEO under accession GSE132939.

862

863 Custom analysis scripts used in this study are available in the GitHub repository

864 <https://github.com/schmitzlab/somatic-epigenetic-mutation-poplar>.

865

866 **Competing interests**

867

868 The authors declare that they have no competing interests.

869

870 **Funding**

871

872 This study was supported by the National Science Foundation (IOS-1546867) to RJS
873 and JS and the National Institutes of Health (R01-GM134682) to RJS and DWH. FJ and
874 RJS acknowledge support from the Technical University of Munich-Institute for
875 Advanced Study funded by the German Excellent Initiative and the European Seventh
876 Framework Programme under grant agreement no. 291763. FJ is also supported by the
877 SFB/Sonderforschungsbereich924 of the Deutsche Forschungsgemeinschaft (DFG).
878 RJS is a Pew Scholar in the Biomedical Sciences, supported by The Pew Charitable
879 Trusts. BTH was supported by the National Institute of General Medical Sciences of the
880 National Institutes of Health (T32GM007103). The work conducted by the U.S.
881 Department of Energy Joint Genome Institute is supported by the Office of Science of
882 the U.S. Department of Energy under Contract No. DE-AC02-05CH11231. Sequencing
883 in this project was partially supported by a JGI community sequencing project grant
884 CSP1678 to RS and GAT.

885

886 **Authors' Contributions**

887

888 RJS, FJ, GAT, RS and JS conceived and designed the experiments. JG, SS, KB, KL,
889 CA, AL, DK, JT, RW performed data generation. BTH, JD, MCT, YS, RH, SM, JJ, PPG,
890 FJ performed data analysis. BTH prepared the figures and manuscript. BTH, DWH,
891 GAT, FJ, and RJS wrote and revised the manuscript with input from all authors. All
892 authors read and approved the final manuscript.

893

894 **Acknowledgements**

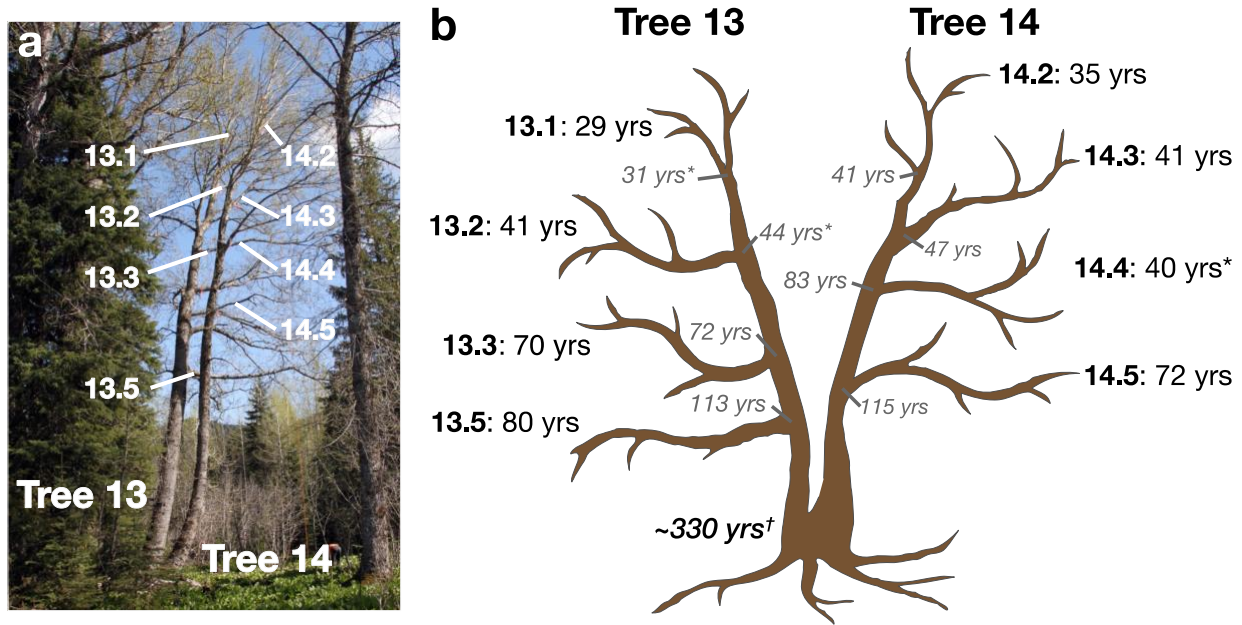
895

896 We thank the JGI and collaborators for pre-publication access to *P. trichocarpa* v4.0
897 genome sequence for chromosome scale ordering of the *Stettler* genome and use of
898 the RNA-seq data from the JGI Plant Gene Atlas for annotation. Sample collection was
899 supported by the Center for Bioenergy Innovation (CBI). CBI is Bioenergy Research
900 Centers supported by the Office of Biological and Environmental Research in the US
901 Department of Energy Office of Science. We also thank Dr. Pankaj Jaiswal for use of
902 additional RNA-seq data included in the annotation.

903

904 **FIGURES**

905



906

907

908 **Fig. 1. Photograph and schematic drawing of Tree 13 and Tree 14.** This wild *P.*

909 *trichocarpa*, located near Mt. Hood, Oregon, experienced a decapitation event ~300

910 years ago. Tree 14 re-sprouted from the stump and ~80-100 years later Tree 13 re-

911 sprouted. (a) Leaf samples were collected from the labeled terminal branches. (b) Age

912 was estimated for both the end of the branch (black font) and where it meets the main

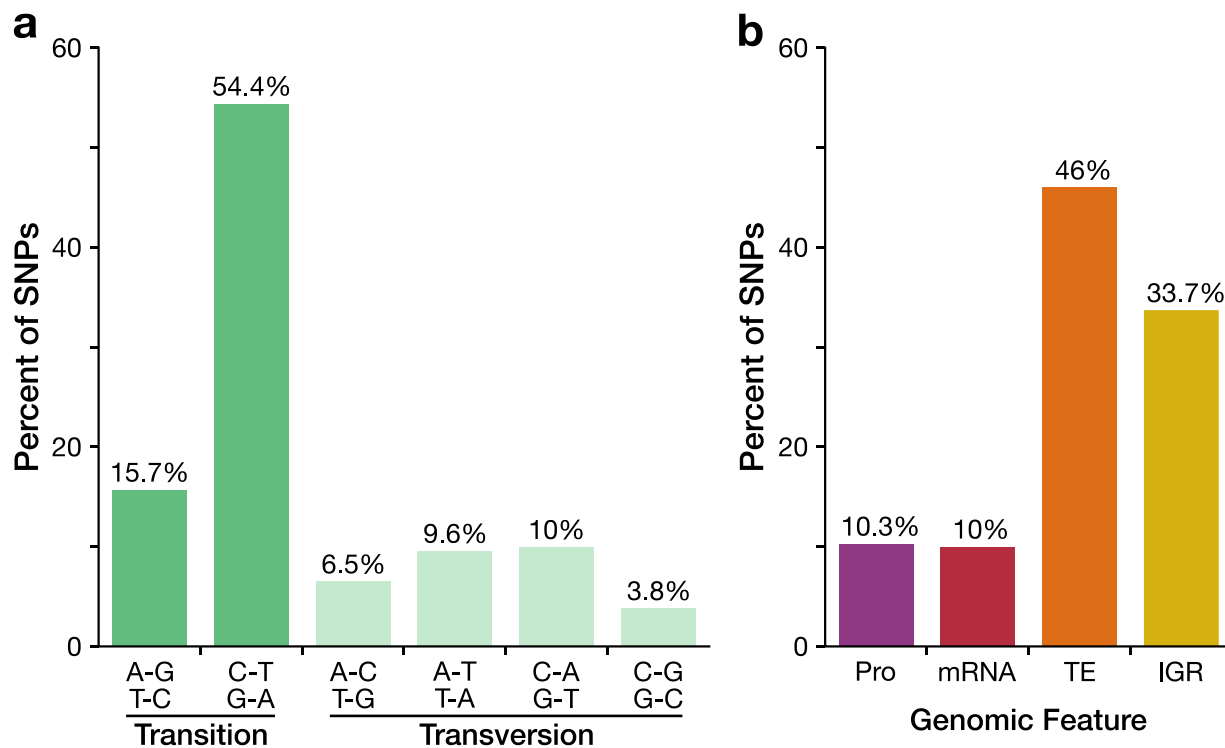
913 stem (gray italics). Ages with * indicate age was estimated using diameter; all other

914 estimates were from core samples. Leaf samples of each branch was used to create

915 genomic sequencing libraries, PacBio libraries, whole-genome bisulfite sequencing

916 libraries, and mRNA-sequencing libraries.

917



918

919

920 **Fig. 2. Most somatic mutations are transitions and occur in non-genic regions. (a)**

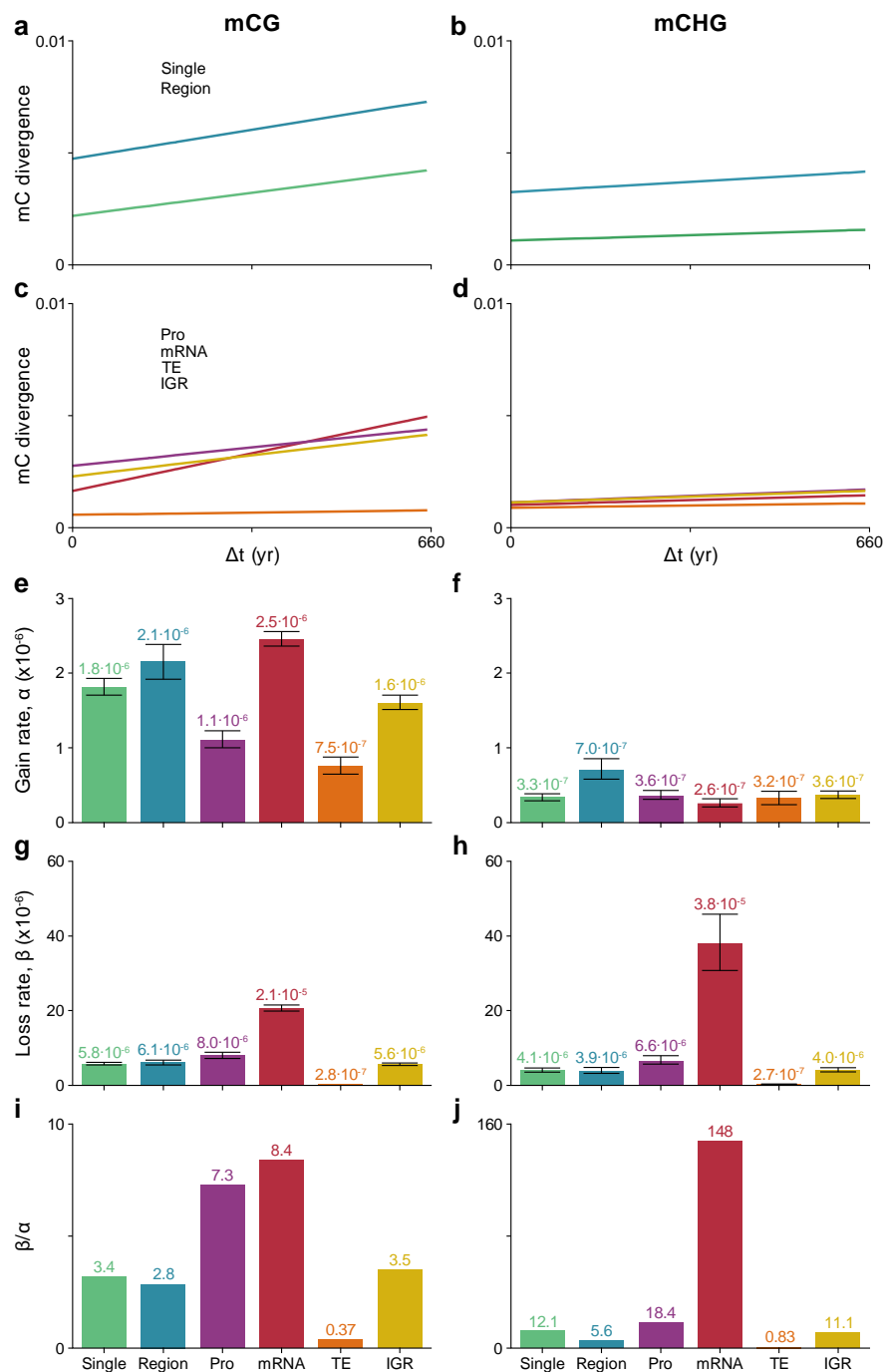
921 Distribution of reference to alternative allele observed in the high-confidence SNPs

922 identified in Tree 13 and Tree 14. (b) Distribution of high-confidence SNPs separated by

923 the genomic feature. Abbreviations: Pro, promoter; 2 kb upstream of TSS; TE,

924 transposable elements and repeats; and IGR, intergenic regions.

925

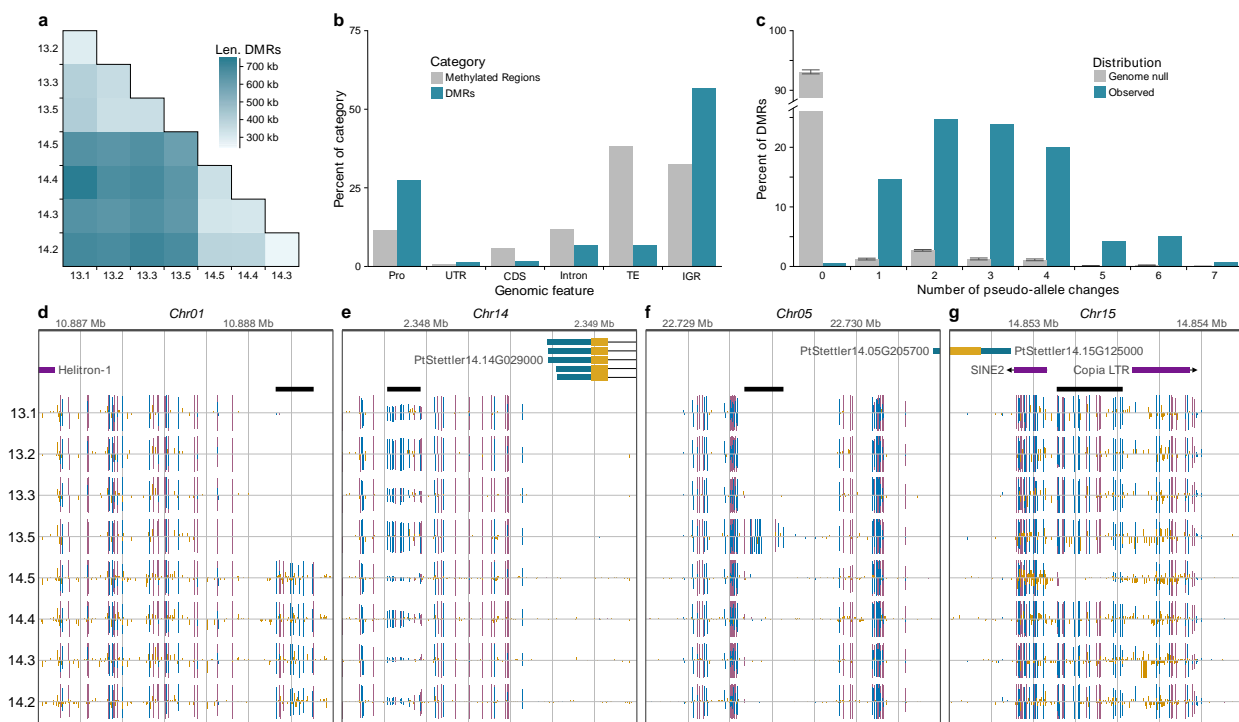


926

927

928 **Fig. 3. Somatic epimutation rates for single sites, regions, and by genomic**
 929 **feature.** mCG (a) and mCHG (b) divergence by branch time divergence for single sites
 930 and regions; mCG (c) and mCHG (d) divergence by branch time divergence for

931 genomic features Pro (promoter; 2 kb upstream of TSS), mRNA, TE (transposable
 932 elements), and IGR (intergenic regions); Estimated mCG (e) and mCHG (f) gain rates
 933 by feature; Estimated mCG (g) and mCHG (h) loss rates by feature; Ratio of mCG (i)
 934 and mCHG (j) loss to gain by feature. Error bars represent bootstrapped 95%
 935 confidence intervals of the estimates. Abbreviations: Pro, promoter; 1.5 kb upstream of
 936 TSS; TE, transposable elements and repeats; and IGR, intergenic regions.
 937



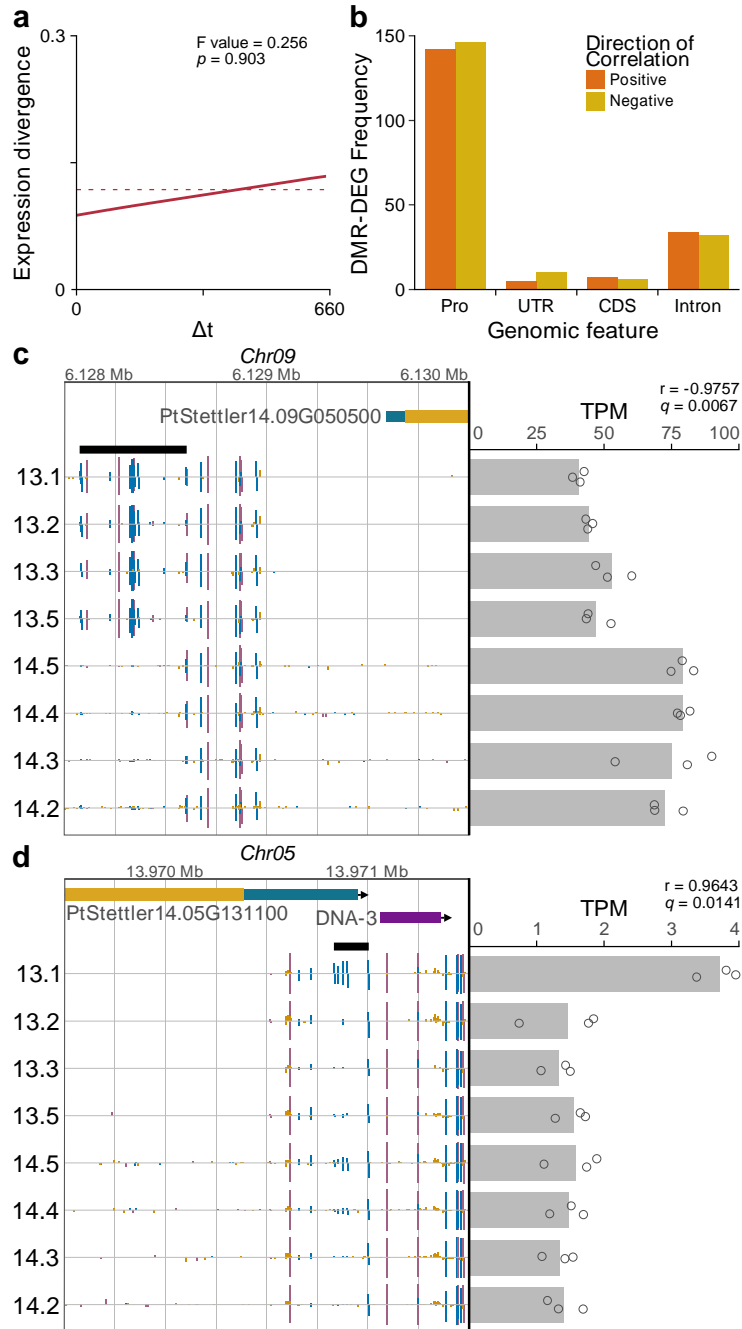
938

939

940 **Fig. 4. Identification and quantification of somatic stability of differentially**

941 **methylated regions.** (a) Divergence of differentially methylated regions corresponds to
 942 divergence in age. The darker color indicates combined length of the pairwise DMRs;
 943 (b) The genome-wide distribution of identified DMRs in genomic features. Abbreviations:
 944 TE, transposable elements and repeats; IGR, intergenic region; Pro, promoter region (2

945 kb upstream of transcription start site); UTR, untranslated regions; CDS, coding
946 sequence. Methylated regions were identified in as regions methylated in at least one
947 sample. (c) There are significantly more pseudo-allele changes between the branches
948 at DMRs (blue) compared to the genome-wide null (Wilcox rank sum, one-sided, P
949 value $< 2 \times 10^{-16}$). Gray bars are the genome-wide null as mean \pm std. dev. across 10
950 simulations. (d) Browser screenshot of a tree specific DMR where all branches in tree
951 13 are homozygous unmethylated and all branches of tree 14 are homozygous
952 methylated. (e) Browser screenshot of a highly variable DMR where the pseudo allele
953 state changes between each branch. (f) Browser screenshot of a single gain DMR
954 where all branches except 13.5 are homozygous unmethylated and 13.5 gains
955 methylation. (g) Browser screenshot of a single loss DMR where all branches except
956 14.5 are homozygous methylated and 14.5 has lost methylation. For d-g, gene models
957 and transposable elements are shown at the top and methylome tracks are below.
958 Vertical bars indicate methylation at the position, where height corresponds to level and
959 color is context, red for CG, blue for CHG, and yellow for CHH. DMR is indicated by
960 thick black horizontal line.
961



962

963

964 **Fig. 5. Gene expression is largely independent from divergence age and nearby**

965 **cytosine methylation except in a few examples.** a) Gene expression divergence is

966 not significantly associated with divergence age. b) Distribution of positive and negative

967 correlations for differentially expressed genes and overlapping/nearby DMRs. Positive

968 correlation occurs when the higher methylation level is associated with higher gene
969 expression among the samples. (c) A significantly negatively correlated, tree-specific
970 DMR and DEG where the DMR occurs in the promoter region of the gene (Pearson's
971 correlation test, two-sided, $N = 8$, adjusted P value = 0.0067). The higher methylation
972 levels in the DMR for tree 13 branches are associated with lower gene expression. (d) A
973 significantly positively correlated, single gain DMR and DEG where the DMR occurs in
974 the 5' untranslated region of the gene (Pearson's correlation test, two-sided, $N = 8$,
975 adjusted $P = 0.0141$). The higher methylation level in the DMR for branch 13.1 is
976 associated with greater gene expression. For c and d, gene expression, as transcripts
977 per million (TPM), is represented as points for the individual replicates and as bar for
978 mean among replicates. In the genome browser view, gene models and transposable
979 elements are shown at the top and methylome tracks are below. Vertical bars indicate
980 methylation at the position, where height corresponds to level and color is context, red
981 for CG, blue for CHG, and yellow for CHH. DMR is indicated by thick black horizontal
982 line.

983

984 REFERENCES

985

- 986 1. Whitham TG, Slobodchikoff CN. Evolution by individuals, plant-herbivore
987 interactions, and mosaics of genetic variability: The adaptive significance of
988 somatic mutations in plants. *Oecologia*. 1981; 49: 287.
- 989 2. Walbot V. On the life strategies of plants and animals. *Trends in Genetics*. 1985;
990 doi:10.1016/0168-9525(85)90071-X.

- 991 3. Gill DE. Individual plants as genetic mosaics: Ecological organisms versus
992 evolutionary individuals. In: Crawley MJ, editor. *Plant Ecology*. Oxford: Blackwell
993 Scientific Publications; 1986. p. 321-343.
- 994 4. Gill DE, Chao L, Perkins SL, Wolf JB. Genetic mosaicism in plants and clonal
995 animals. *Annual review of Ecology and Systematics*. 1995; 26: 423-444.
- 996 5. Hadany L. A conflict between two evolutionary levels in trees. *J Theor Biol*. 2001
997 Feb 21; doi:10.1006/jtbi.2000.2236.
- 998 6. Clarke E. Plant individuality and multilevel selection theory. The major transitions in
999 evolution revisited. 2011; 227-250.
- 1000 7. Folse III HJ, Roughgarden J. Direct benefits of genetic mosaicism and
1001 intraorganismal selection: modeling coevolution between a long-lived tree and a
1002 short-lived herbivore. *Evolution: International Journal of Organic Evolution*. 2012;
1003 66: 1091-1113.
- 1004 8. Tuskan GA, Groover AT, Schmutz J, DiFazio SP, Myburg A, Grattapaglia D et al.
1005 *Hardwood Tree Genomics: Unlocking Woody Plant Biology*. *Frontiers in Plant*
1006 *Science*. 2018; doi:10.3389/fpls.2018.01799.
- 1007 9. Padovan A, Keszey A, Foley WJ, K^olheim C. Differences in gene expression
1008 within a striking phenotypic mosaic Eucalyptustree that varies in susceptibility to
1009 herbivory. *BMC Plant Biology*. 2013; doi:10.1186/1471-2229-13-29.
- 1010 10. Wen I-C, Koch KE, Sherman WB. Comparing Fruit and Tree Characteristics of
1011 Two Peaches and Their Nectarine Mutants. *J Amer Soc Hort Sci*. 1995;
1012 doi:10.21273/JASHS.120.1.101.

- 1013 11. Laucou V, Lacombe T, Dechesne F, Siret R, Bruno J-P, Dessup M et al. High
1014 throughput analysis of grape genetic diversity as a tool for germplasm collection
1015 management. *Theor Appl Genet.* 2011; doi:10.1007/s00122-010-1527-y.
- 1016 12. Tuskan GA, Francis KE, Russ SL, Romme WH, Turner MG. RAPD markers reveal
1017 diversity within and among clonal and seedling stands of aspen in Yellowstone
1018 National Park, U.S.A. *Can J For Res.* 1996; doi:10.1139/x26-237.
- 1019 13. Diwan D, Komazaki S, Suzuki M, Nemoto N, Aita T, Satake A et al. Systematic
1020 genome sequence differences among leaf cells within individual trees. *BMC*
1021 *genomics.* 2014; 15: 142.
- 1022 14. Schmid-Siegert E, Sarkar N, Iseli C, Calderon S, Gouhier-Darimont C, Chrast J et
1023 al. Low number of fixed somatic mutations in a long-lived oak tree. *Nat Plants.*
1024 2017 Dec; doi:10.1038/s41477-017-0066-9.
- 1025 15. Plomion C, Aury J-M, Amselem J, Leroy T, Murat F, Duplessis S et al. Oak
1026 genome reveals facets of long lifespan. *Nat Plants.* 2018 07; doi:10.1038/s41477-
1027 018-0172-3.
- 1028 16. Ossowski S, Schneeberger K, Lucas-Lledö JI, Warthmann N, Clark RM, Shaw RG
1029 et al. The rate and molecular spectrum of spontaneous mutations in *Arabidopsis*
1030 *thaliana.* *Science.* 2010; 327: 92-94.
- 1031 17. Groot EP, Laux T. Ageing: How Do Long-Lived Plants Escape Mutational
1032 Meltdown. *Curr Biol.* 2016 07 11; doi:10.1016/j.cub.2016.05.049.
- 1033 18. Wang L, Ji Y, Hu Y, Hu H, Jia X, Jiang M et al. The architecture of intra-organism
1034 mutation rate variation in plants. *PLoS biology.* 2019; 17: e3000191.

- 1035 19. Burian A, Barbier de Reuille P, Kuhlemeier C. Patterns of Stem Cell Divisions
1036 Contribute to Plant Longevity. *Current Biology*. 2016;
1037 doi:10.1016/j.cub.2016.03.067.
- 1038 20. Klekowski EJ, Godfrey PJ. Ageing and mutation in plants. *Nature*. 1989;
1039 doi:10.1038/340389a0.
- 1040 21. Bobiwash K, Schultz ST, Schoen DJ. Somatic deleterious mutation rate in a woody
1041 plant: estimation from phenotypic data. *Heredity*. 2013; 111: 338.
- 1042 22. Schmitz RJ, Schultz MD, Urich MA, Nery JR, Pelizzola M, Libiger O et al. Patterns
1043 of population epigenomic diversity. *Nature*. 2013 Mar 14; doi:10.1038/nature11968.
- 1044 23. Calarco JP, Borges F, Donoghue MT, Van Ex F, Jullien PE, Lopes T et al.
1045 Reprogramming of DNA methylation in pollen guides epigenetic inheritance via
1046 small RNA. *Cell*. 2012 Sep 28; doi:10.1016/j.cell.2012.09.001.
- 1047 24. Law JA, Jacobsen SE. Establishing, maintaining and modifying DNA methylation
1048 patterns in plants and animals. *Nat Rev Genet*. 2010 Mar; doi:10.1038/nrg2719.
- 1049 25. Johannes F, Schmitz RJ. Spontaneous epimutations in plants. *New Phytol*. 2019
1050 Feb; doi:10.1111/nph.15434.
- 1051 26. Cubas P, Vincent C, Coen E. An epigenetic mutation responsible for natural
1052 variation in floral symmetry. *Nature*. 1999; 401: 157-161.
- 1053 27. Manning K, Tör M, Poole M, Hong Y, Thompson AJ, King GJ et al. A naturally
1054 occurring epigenetic mutation in a gene encoding an SBP-box transcription factor
1055 inhibits tomato fruit ripening. *Nat Genet*. 2006 Aug; doi:10.1038/ng1841.

- 1056 28. Ong-Abdullah M, Ordway JM, Jiang N, Ooi S-E, Kok S-Y, Sarpan N et al. Loss of
1057 Karma transposon methylation underlies the mantled somaclonal variant of oil
1058 palm. *Nature*. 2015; 525: 533-537.
- 1059 29. Schmitz RJ, Schultz MD, Lewsey MG, O'Malley RC, Urich MA, Libiger O et al.
1060 Transgenerational epigenetic instability is a source of novel methylation variants.
1061 *Science*. 2011; doi:DOI: 10.1126/science.1212959.
- 1062 30. Becker C, Hagemann J, Müller J, Koenig D, Stegle O, Borgwardt K et al.
1063 Spontaneous epigenetic variation in the *Arabidopsis thaliana* methylome. *Nature*.
1064 2011 Dec 8; doi:10.1038/nature10555.
- 1065 31. Hofmeister BT, Lee K, Rohr NA, Hall DW, Schmitz RJ. Stable inheritance of DNA
1066 methylation allows creation of epigenotype maps and the study of epiallele
1067 inheritance patterns in the absence of genetic variation. *Genome Biol*. 2017 Aug
1068 16; doi:10.1186/s13059-017-1288-x.
- 1069 32. van der Graaf A, Wardenaar R, Neumann DA, Taudt A, Shaw RG, Jansen RC et
1070 al. Rate, spectrum, and evolutionary dynamics of spontaneous epimutations. *Proc*
1071 *Natl Acad Sci U S A*. 2015 May 11; doi:10.1073/pnas.1424254112.
- 1072 33. Heer K, Ullrich KK, Hiss M, Liepelt S, Schulze Brüning R, Zhou J et al. Detection of
1073 somatic epigenetic variation in Norway spruce via targeted bisulfite sequencing.
1074 *Ecology and Evolution*. 2018; doi:10.1002/ece3.4374.
- 1075 34. Liang D, Zhang Z, Wu H, Huang C, Shuai P, Ye C-Y et al. Single-base-resolution
1076 methylomes of *Populus trichocarpa* reveal the association between DNA
1077 methylation and drought stress. *BMC Genet*. 2014; doi:10.1186/1471-2156-15-S1-
1078 S9.

- 1079 35. Su Y, Bai X, Yang W, Wang W, Chen Z, Ma J et al. Single-base-resolution
1080 methylomes of *Populus euphratica* reveal the association between DNA
1081 methylation and salt stress. *Tree Genetics & Genomes*. 2018; doi:10.1007/s11295-
1082 018-1298-1.
- 1083 36. Le Gac AL, Lafon-Placette C, Chauveau D, Segura V, Delaunay A, Fichot R et al.
1084 Winter-dormant shoot apical meristem in poplar trees shows environmental
1085 epigenetic memory. *J Exp Bot*. 2018 Sep 14; doi:10.1093/jxb/ery271.
- 1086 37. Xiao CL, Chen Y, Xie SQ, Chen KN, Wang Y, Han Y et al. MECAT: fast mapping,
1087 error correction, and de novo assembly for single-molecule sequencing reads. *Nat*
1088 *Methods*. 2017 Nov; doi:10.1038/nmeth.4432.
- 1089 38. Chin CS, Alexander DH, Marks P, Klammer AA, Drake J, Heiner C et al.
1090 Nonhybrid, finished microbial genome assemblies from long-read SMRT
1091 sequencing data. *Nat Methods*. 2013 Jun; doi:10.1038/nmeth.2474.
- 1092 39. Ingvarsson PK. Multilocus patterns of nucleotide polymorphism and the
1093 demographic history of *Populus tremula*. *Genetics*. 2008;
1094 doi:10.1534/genetics.108.090431.
- 1095 40. Rood SB, Polzin ML. Big old cottonwoods. *Can J Bot*. 2003; 81: 764-767.
- 1096 41. Schultz MD, Schmitz RJ, Ecker JR. 'Leveling' the playing field for analyses of
1097 single-base resolution DNA methylomes. *Trends Genet*. 2012 Dec;
1098 doi:10.1016/j.tig.2012.10.012.
- 1099 42. Bewick AJ, Ji L, Niederhuth CE, Willing E-M, Hofmeister BT, Shi X et al. On the
1100 origin and evolutionary consequences of gene body DNA methylation. *PNAS*.
1101 2016; doi:10.1073/pnas.1604666113.

- 1102 43. Wendte JM, Zhang Y, Ji L, Shi X, Hazarika RR, Shahryary Y et al. Epimutations
1103 are associated with CHROMOMETHYLASE 3-induced de novo DNA methylation.
1104 eLife. 2019; doi:10.7554/elife.47891.001.
- 1105 44. Melquist S, Luff B, Bender J. Arabidopsis PAI gene arrangements, cytosine
1106 methylation and expression. Genetics. 1999; 153: 401-413.
- 1107 45. Silveira AB, Trontin C, Cortijo S, Barau J, Del Bem LE, Loudet O et al. Extensive
1108 natural epigenetic variation at a de novo originated gene. PLoS Genet. 2013 Apr;
1109 doi:10.1371/journal.pgen.1003437.
- 1110 46. Love MI, Huber W, Anders S. Moderated estimation of fold change and dispersion
1111 for RNA-seq data with DESeq2. Genome Biology. 2014; doi:10.1186/s13059-014-
1112 0550-8.
- 1113 47. Narsai R, Gouil Q, Secco D, Srivastava A, Karpievitch YV, Liew LC et al. Extensive
1114 transcriptomic and epigenomic remodelling occurs during Arabidopsis thaliana
1115 germination. Genome Biol. 2017 09 15; doi:10.1186/s13059-017-1302-3.
- 1116 48. Kawakatsu T, Nery JR, Castanon R, Ecker JR. Dynamic DNA methylation
1117 reconfiguration during seed development and germination. Genome Biol. 2017 09
1118 15; doi:10.1186/s13059-017-1251-x.
- 1119 49. Lin JY, Le BH, Chen M, Henry KF, Hur J, Hsieh TF et al. Similarity between
1120 soybean and Arabidopsis seed methylomes and loss of non-CG methylation does
1121 not affect seed development. Proc Natl Acad Sci U S A. 2017 11 07;
1122 doi:10.1073/pnas.1716758114.

- 1123 50. Bouyer D, Kramdi A, Kassam M, Heese M, Schnittger A, Roudier F et al. DNA
1124 methylation dynamics during early plant life. *Genome Biol.* 2017 09 25;
1125 doi:10.1186/s13059-017-1313-0.
- 1126 51. Ji L, Mathioni SM, Johnson S, Tucker D, Bewick AJ, Do Kim K et al. Genome-wide
1127 reinforcement of DNA methylation occurs during somatic embryogenesis in
1128 soybean. *The Plant Cell.* 2019; 31: 2315-2331.
- 1129 52. Deflorio G, Hein S, Fink S, Spiecker H, Willis Mathew Robert Schwarze F. The
1130 application of wood decay fungi to enhance annual ring detection in three diffuse-
1131 porous hardwoods. *Dendrochronologia.* 2005; doi:10.1016/j.dendro.2005.02.002.
- 1132 53. DeRose JR, Gardner RS. Technique to improve visualization of elusive tree-ring
1133 boundaries in aspen (*Populus tremuloides*). *Tree-Ring Research.* 2010; 66: 75-79.
- 1134 54. Li H. Aligning sequence reads, clone sequences and assembly contigs with BWA-
1135 MEM. arXiv preprint arXiv:13033997. 2013;
- 1136 55. McKenna A, Hanna M, Banks E, Sivachenko A, Cibulskis K, Kernytsky A et al. The
1137 Genome Analysis Toolkit: a MapReduce framework for analyzing next-generation
1138 DNA sequencing data. *Genome research.* 2010; 20: 1297-1303.
- 1139 56. Haas BJ, Delcher AL, Mount SM, Wortman JR, Smith RK, Hannick LI et al.
1140 Improving the Arabidopsis genome annotation using maximal transcript alignment
1141 assemblies. *Nucleic Acids Res.* 2003 Oct 01; doi:10.1093/nar/gkg770.
- 1142 57. Smit AFA, Hubley R, Green P. RepeatMasker Open-4.0. 2013–2015.
1143 <http://www.repeatmasker.org>.
- 1144 58. Salamov AA, Solovyev VV. Ab initio gene finding in Drosophila genomic DNA.
1145 *Genome research.* 2000; 10: 516-522.

- 1146 59. Slater GSC, Birney E. Automated generation of heuristics for biological sequence
1147 comparison. *BMC bioinformatics*. 2005; 6: 31.
- 1148 60. Hoff KJ, Lange S, Lomsadze A, Borodovsky M, Stanke M. BRAKER1:
1149 unsupervised RNA-Seq-based genome annotation with GeneMark-ET and
1150 AUGUSTUS. *Bioinformatics*. 2015; 32: 767-769.
- 1151 61. Li H, Handsaker B, Wysoker A, Fennell T, Ruan J, Homer N et al. The sequence
1152 alignment/map format and SAMtools. *Bioinformatics*. 2009;
1153 doi:10.1093/bioinformatics/btp352.
- 1154 62. Koboldt DC, Zhang Q, Larson DE, Shen D, McLellan MD, Lin L et al. VarScan 2:
1155 somatic mutation and copy number alteration discovery in cancer by exome
1156 sequencing. *Genome Res*. 2012 Mar; doi:10.1101/gr.129684.111.
- 1157 63. Martin ER, Kinnamon DD, Schmidt MA, Powell EH, Zuchner S, Morris RW.
1158 SeqEM: an adaptive genotype-calling approach for next-generation sequencing
1159 studies. *Bioinformatics*. 2010 Nov 15; doi:10.1093/bioinformatics/btq526.
- 1160 64. Sedlazeck FJ, Rescheneder P, Smolka M, Fang H, Nattestad M, von Haeseler A et
1161 al. Accurate detection of complex structural variations using single-molecule
1162 sequencing. *Nat Methods*. 2018 06; doi:10.1038/s41592-018-0001-7.
- 1163 65. Benson G. Tandem repeats finder: a program to analyze DNA sequences. *Nucleic
1164 Acids Res*. 1999 Jan 15; doi:10.1093/nar/27.2.573.
- 1165 66. Team RC. R: A Language and Environment for Statistical Computing. Vienna,
1166 Austria: R Foundation for Statistical Computing; 2016. p.
- 1167 67. Robinson JT, Thorvaldsdóttir H, Winckler W, Guttman M, Lander ES, Getz G et al.
1168 Integrative genomics viewer. *Nature biotechnology*. 2011; 29: 24-26.

- 1169 68. Urich MA, Nery JR, Lister R, Schmitz RJ, Ecker JR. MethylC-seq library
1170 preparation for base-resolution whole-genome bisulfite sequencing. *Nat Protoc.*
1171 2015 Mar; doi:10.1038/nprot.2014.114.
- 1172 69. Schultz MD, He Y, Whitaker JW, Hariharan M, Mukamel EA, Leung D et al. Human
1173 body epigenome maps reveal noncanonical DNA methylation variation. *Nature.*
1174 2015 Jul 9; doi:10.1038/nature14465.
- 1175 70. Benjamini Y, Hochberg Y. Controlling the false discovery rate: a practical and
1176 powerful approach to multiple testing. *Journal of the Royal statistical society: series*
1177 *B (Methodological)*. 1995; 57: 289-300.
- 1178 71. Quinlan AR, Hall IM. BEDTools: a flexible suite of utilities for comparing genomic
1179 features. *Bioinformatics*. 2010; 26: 841-842.
- 1180 72. Bolger AM, Lohse M, Usadel B. Trimmomatic: a flexible trimmer for Illumina
1181 sequence data. *Bioinformatics*. 2014 Aug 1; doi:10.1093/bioinformatics/btu170.
- 1182 73. Kim D, Langmead B, Salzberg SL. HISAT: a fast spliced aligner with low memory
1183 requirements. *Nat Methods*. 2015 Apr; doi:10.1038/nmeth.3317.
- 1184 74. Perteza M, Perteza GM, Antonescu CM, Chang TC, Mendell JT, Salzberg SL.
1185 StringTie enables improved reconstruction of a transcriptome from RNA-seq reads.
1186 *Nat Biotechnol*. 2015 Mar; doi:10.1038/nbt.3122.
- 1187